

Article citation info:

Studziński R, Sumelka W, Malendowski M, Gajewski T, Al-Rifaie H, Sielicki P, Sandwich panel subjected to blast wave impact and accelerated fragments, *Eksploracja i Niezawodność – Maintenance and Reliability* 2024: 26(2) <http://doi.org/10.17531/ein/183698>

## Sandwich panel subjected to blast wave impact and accelerated fragments

Indexed by:



Robert Studziński<sup>a,\*</sup>, Wojciech Sumelka<sup>a</sup>, Michał Malendowski<sup>a</sup>, Tomasz Gajewski<sup>a</sup>, Hasan Al-Rifaie<sup>a</sup>, Piotr Sielicki<sup>a</sup>

<sup>a</sup> Faculty of Civil and Transport Engineering, Poznan University of Technology, Poland

### Highlights

- Sandwich panels – metallic thin faces, PIR core – have poor antipenetration abilities.
- Equivalent static load is reliable for global analysis of sandwich panels.
- The 3-stage FE approach is reliable for investigating an obstacle subjected to blast load.

### Abstract

The article presents sandwich panels subjected to blast wave impact and accelerated fragments. The research discusses results obtained from original experimental setups that fill a gap in the area of investigation of the mechanical response of sandwich panels used in civil engineering applications under accidental design situations such as blast wave impact and/or fragment penetration. In field experiments, a high-speed camera was used to record both the fragment trajectory and the deflection of the sandwich panel. The authors proposed the equivalent static load for both the global analysis of the sandwich panel and the calibration of the numerical model. In FE modelling, CONWEP algorithm was used to simulate blast wave impact, and ductile damage model material to allow perforation of the sandwich panel faces. The convergence of mesh size was analyzed. For the validated numerical model, an evaluation of the effect of the size of the fragment (diameter/mass) on the outlet velocity and the size of the inlet and outlet holes was carried out.

### Keywords

impact load, fragment penetration, fragment velocity, equivalent static load, failure mechanisms

This is an open access article under the CC BY license (<https://creativecommons.org/licenses/by/4.0/>)

### 1. Introduction

The paper presents original research which fills the gap in the area of the reliability assessment of wall cladding sandwich panels subjected to blast load and accelerated fragments. The article also presents the authors' test bed that allows for simultaneous simulation of the wave impact load and the fragment penetration. In the experiments, the fragments represented by steel spherical bullets were accelerated by the wave impact. The investigation of fragment penetration can be addressed to an accidental design situation where the danger of improvised explosive devices [23] had to be assessed.

Investigated sandwich panels are, in fact, three layered composite elements – two thin (about 0.5mm in thickness) external faces and thick (from 60mm to 200mm in thickness) core in between. Note that in building applications, Young's modulus of thin external faces is approximately 40 thousand times higher than Young's modulus of the core [30]. Therefore, from a mechanical point of view, the thick and soft core transfers the shear stresses and provides an appropriate distance for the thin and stiff external facings.

The fact that only a few research groups have focused on the

(\* ) Corresponding author.

E-mail addresses:

R. Studziński (ORCID: 0000-0002-0906-8701) [robert.studzinski@put.poznan.pl](mailto:robert.studzinski@put.poznan.pl), W. Sumelka (ORCID: 0000-0002-8317-748X) [wojciech.sumelka@put.poznan.pl](mailto:wojciech.sumelka@put.poznan.pl), M. Malendowski, (ORCID: 0000-0002-2698-8358) [michal.malendowski@put.poznan.pl](mailto:michal.malendowski@put.poznan.pl), T. Gajewski (ORCID: 0000-0002-4292-0417) [tomasz.gajewski@put.poznan.pl](mailto:tomasz.gajewski@put.poznan.pl), H. Al-Rifaie (ORCID: 0000-0002-2984-1247) [hasan.al-rifaie@put.poznan.pl](mailto:hasan.al-rifaie@put.poznan.pl), P. Sielicki (ORCID: 0000-0002-5331-6645) [piotr.sielicki@put.poznan.pl](mailto:piotr.sielicki@put.poznan.pl),

blast resistance of sandwich panels used in structural building engineering does not mean that these panels cannot be exposed to a wave impact load when used in building applications. For example, such panels might experience a potential wave impact load from the accidental explosion of technical gases stored in cylinders [21]. In the subject literature, sandwich panels subjected to air or underwater blast loading are considered energy-absorbent or sacrificial cladding elements [29]. Such panels typically consist of metallic external facings and a metallic or polymeric foam core. The ability to absorb the energy from a blast or impact load has been investigated in core layer modifications rather than facing modifications. Therefore, one direction of this research involves a layer-gradient core. In the publication [33], square and fixed-along-four-edges sandwich panels with a three-layer metal foam core were subjected to air blast loading. Zhou and Jing in [33] developed an analytical expression for maximal deflection using the new yield criterion for sandwich panels with three-layered cores. Furthermore, experiments and numerical simulations verified the accuracy of this analytical approach. In the publication [16], an experimental investigation revealed that a stepwise density core reduced sandwich panel deflection. In that approach, an underwater blast load subjects a sandwich panel with glass-fibre-reinforced polymer facings. Although [5] also investigated different densities along the core layer made of extruded polystyrene (XPS). The introduction of the Deshpande–Fleck model for the foam core allowed researchers to correlate well with the finite element model and the experiment. Brekken et al. in [16] recommended the use of this approach for simulation-based optimisation of sandwich panels with XPS core layer subjected to blast loading.

The ability to absorb energy is also an important parameter, for example, while investigating the stiffness of a military vehicle subjected to an explosion of a landmine or improvised explosive device (IED). In [10], the method of evaluating the stiffness of a vehicle with respect to the risk of such explosion is presented. Composite structures are also used in aviation. In [12], the fibre reinforced composites, which were subjected to low-energy impact load, are discussed. It was presented there that, in the case of aircraft made of composites, the safety of the flight may be endangered even by the impact of a very low energy. The composites made of polymer-glass were

investigated in [24] to assess their functional usability for ballistic shield plates. Also the aspect of the energy absorption is important while impact loads are considered [8, 9].

The second direction of the research topic concerns sandwich panels with various configurations of a metallic lattice core. In [6], the mechanical response of sandwich panels with a tubular core subjected to blast load was investigated. This research involved parametric studies of various tube spacings and different arrangements of various materials. The following four configurations of a sandwich panel core layer made of the corrugated metal plate were experimentally investigated by [32]: corrugated core without polymeric foam; corrugated core with polymeric foam in the top folds; corrugated core with polymeric foam in the bottom folds; and corrugated core with polymeric foam in the top and bottom folds. In the publication [2], different lattice core layer configurations were considered in finite element simulation of sandwich panels subjected to a blast load. In that investigation, the ability to dissipate energy from the blast load through the plastic deformations of the core layer of the sandwich panel was compared using performance indicators. The publications [3, 4] present experimental and numerical results for sandwich panels (considered sacrificial elements) with various unconnected corrugated core layers made of aluminium. One of the outcomes of this research was the conclusion that this type of sandwich panel should not be considered a protection element in the case of close-in detonation. Next, a metallic I-shaped core layer was examined in [31]. This research compared two types of loading: blast loads with debris ('combined') and blast loads without debris. The effects of a blast load with debris were found to be more severe than those of a blast load without debris. The authors enhanced their experimental results by numerical modelling and obtained a good correlation between the experiment and FE modelling. Another way of improving the energy-absorbing ability of sandwich panels is by optimising their faces. In the publication [22], the change in sandwich panels' kinematical response (deformation and failure modes) with facings made of different materials is presented.

In the publication [11], the research encompasses two blast-load scenarios. The loading scenarios assumed that the blast load was preceded by an impact that involved, on the one hand, a low-speed weight drop and, on the other hand, a high-speed

projectile. The research revealed that after the high-speed projectile, the absorption abilities of the sandwich panel under investigation were higher. The multiple impulsive pressures on a metallic sandwich panel were presented in [7]. Another load scenario worth mentioning was considered by [27]. The sandwich panels were subjected to an impulsive load in the form of the impact of explosively accelerated sand shells. In this research, global behaviour was correctly predicted by the introduced FE model (a model with modified Johnson-Cook constitutive load and the Cockcroft-Latham fracture criterion), while local failure was not.

The above-mentioned sandwich panels can be characterised by the parallel arrangement of the layers. Researchers have also examined the use of sandwich panels with nonparallel layers subjected to blast load. In [19], the response to a blast load of curved sandwich panels made of aluminium facings and core was investigated. Numerical analyzes (the numerical model was verified and validated with experiments) showed that the initial curvature changed the failure modes of the sandwich panels. At the same time in [14], the blast response of aluminium foam sandwich panels with various configurations of a double V-shaped bottom facing was discussed.

### 1.1. Methodology

The paper presents the original results of research on sandwich panels used in structural engineering applications subjected to blast wave impact and accelerated fragments. The sandwich panel samples tested were rectangular in shape with a width-to-length ratio equal to 2. The samples were freely placed on the test bed supports and then subjected to blast wave impact and accelerated fragments. Research has shown that by introducing the equivalent static load and using the well-known first-order shear deformation theory, it is possible to obtain a reliable global analysis of the sandwich panel subjected to blast wave impact. Such an approach to structural analysis is invaluable in the case of, for example, explosion hazards, when a quick but also reliable assessment of the load-bearing capacity of a sandwich panel is necessary.

The paper consists of seven sections. The first section presents a review of the literature. In the second section, the research problem is formulated together with a description of the research stand. In this section, the geometry/size of the

samples, explosive charge, and fragments are presented. Moreover, the assumed blast wave impact scenario is introduced with the information on the analytically determined change in time of pressure of the middle point at the sandwich panel external facing. The third section discusses the impact effect of fragments on the sandwich panel, including the sizes of the inlet and outlet holes, the spread of fragments along the sandwich panel, and their speed after obstacle penetration. Section four describes the kinematical response of the sandwich panel subjected to blast wave impact. In section five, equivalent static load is introduced using the first-order shear deformation theory. Having the equivalent static load, the verification of the ultimate and serviceability limit states is presented. In section six the three stage (equivalent static → explicit dynamic → explicit dynamic with ductile model definition) finite element calculations of whole sandwich panel subjected to blast wave impact are presented. In this section, the numerical experiment verifying the influence of the mass and size of the fragment on its outlet velocity was preceded by the convergence analysis of the mesh size. The conclusions are formulated in section seven.

## 2. Problem formulation

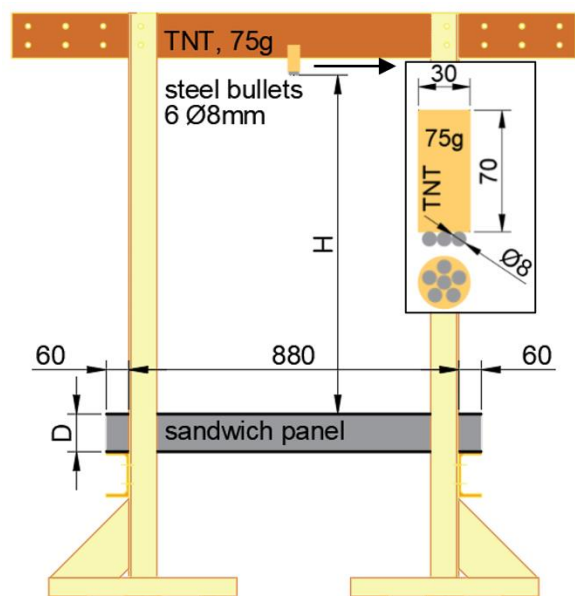


Fig. 1. Testbed scheme and TNT explosive with fragments preparation.

The testbed (see Fig. 1) allows for determining the deformation of the sandwich panel subjected to wave impact load, the spread zones of the fragments, and the flight trajectory and speed of the fragments (before and after perforation of the horizontal

obstacle). In the experiment, a cylindrical explosive charge with 75 g of TNT was used. Six steel spherical bullets were attached in front of the TNT, each 8 mm in diameter and 2.1 g in weight. The attached spherical bullets represent the fragments in the field tests. The cylindrical charge was installed on the steel frame at the specified distance H from the sandwich panel. Note that the sandwich panel was freely (without fasteners) supported on the steel frame beams.

The rectangular sandwich panels (1000 mm in length, 500

mm in width, and 120 mm in nominal thickness) were subjected to blast wave impact. The sandwich panel consisted of two external flat steel facings and a polyisocyanurate core (PIR foam). Table 1 lists the selected geometric measurements and mechanical properties of the sandwich panel layers. It should be emphasised that the steel facings were painted and zinc-coated. The measured coating thickness was about 15% of the nominal thickness of the facing. The stress-strain tensile test of the facings is presented in Section 4.

Table 1. Geometrical measurements and mechanical properties of the sandwich panel facings.

No.	Layer	Measured quantity	Symbols	Units	Mean	Cross-section zoomed $\times 25$
F.1*	Facings	Facing total thickness	$f_F$	[mm]	$0.520 \pm 0.01$	
F.2*		Facing total coating thickness	$t_{F,coat}$	[ $\mu$ m]	$90.0 \pm 6.3$	
F.3*		Yield strength	$f_{yF}$	[MPa]	$377.0 \pm 3.2$	
F.4*		Ultimate strength	$F_{uF}$	[MPa]	$380.8 \pm 6.7$	
F.5*		Young modulus	$E_F$	[GPa]	$190.0 \pm 5.1$	
C.1*	Core	Thickness	$D_C$	[mm]	$119.0 \pm 0.9$	
C.2**		Density	$\rho_C$	[kg/m <sup>3</sup> ]	35.2	
C.3**		Shear modulus	$G_C$	[MPa]	2.9	
C.4**		Shear strength	$f_{vC}$	[kPa]	75.0	

\* data obtained from the author's measurements,  
 \*\* data obtained from sandwich panel producers' declarations

At the site, five tests were carried out on three samples i.e. the experiment assumed multiple trials. The first four tests were conducted for single sandwich panel arrangement, while the fifth was conducted for two stacked sandwich panels (one placed on top of the other). The explosion was designed in free

air, where the shock wave propagated without intermediate amplification; therefore, the blast can be classified as unconfined and spherical. The scheme of use and reuse of sandwich panel samples in the experiments is presented in Fig. 2, while the explosion sequence is depicted in Fig. 3.

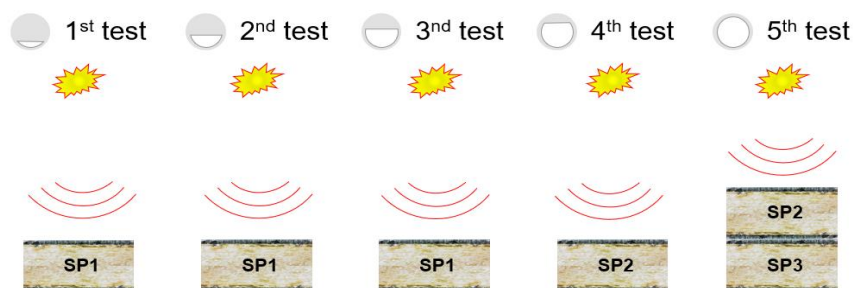


Fig. 2. Arrangement of the sandwich panel samples in tests.

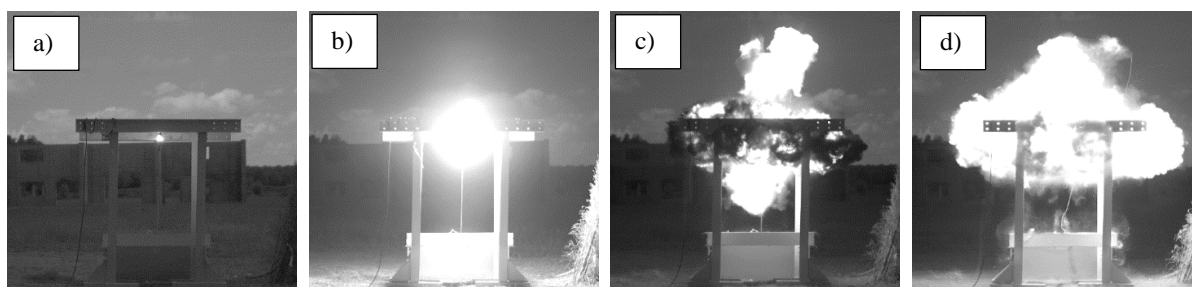


Fig. 3. The sequence of explosion during field tests (description in text).

The following sequences can be distinguished: ignition (see Fig. 3a), a moment of a maximal diameter of the fireball (see Fig. 3b), overpressure phase (see Fig. 3c), and underpressure phase (see Fig. 3d). The frames depicted in Fig. 3 were taken using the high-speed Phantom v2012. The camera is

characterized by a sample rate of 50000 frames per second and a  $640 \times 480$  resolution. Figure 4 shows the change in time of the overpressure of the middle point of the sandwich panel external facing, determined using software for rapid prediction of the wave properties presented in [20].

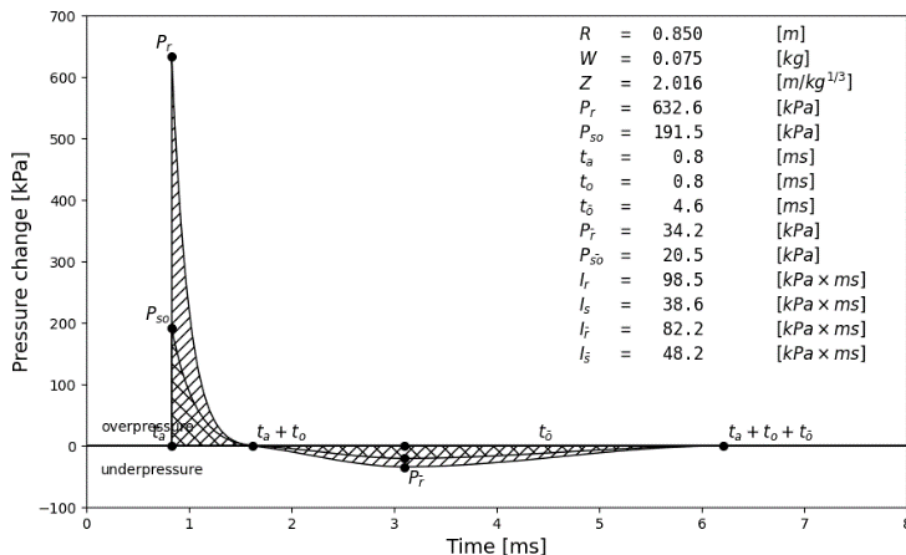


Fig. 4. Change in time of pressure of the middle point of the external facing of a sandwich panel.

Alternatively to the mentioned above software, the readers can use the following approximate analytical procedure to determine a change in time of the overpressure. This procedure, for clarity, can be divided into 7 steps (calculations for  $H = 0.85$  m).

**Step 1:** Find the explosion energy using Eq. 1, where  $Q = 4500$  kJ/kg represents the heat of the explosion for TNT, and  $m = 0.075$  kg represents the mass of the charge

$$E = m \cdot Q = 337.5 \text{ kJ} \quad (1)$$

**Step 2:** Find the equivalent charge radius using Eq. 2. According to Sachs law [17, 26], initial pressure in the medium  $p_0 = 101.6$  kPa taken from the International Standard Atmosphere model

$$r_0 = \left( \frac{E}{\rho_0} \right)^{\frac{1}{3}} = 1.492 \text{ m} \quad (2)$$

**Step 3:** Find the proximity factor using Eq. 3, where  $r = 0.85$  m represents the distance between the unit charge and the external facing of the sandwich panel (in Fig. 1 it is represented by  $H$ ). Note that if  $Z \leq 1.0$  then the explosion is classified as close zone detonation, while if  $Z > 1.0$  then it is classified as a far zone detonation.

$$Z = \frac{r}{\sqrt[3]{m}} = 2.016 \frac{\text{m}}{\sqrt[3]{\text{kg}}} \quad (3)$$

**Step 4:** Find non-dimensional overpressure using the formula proposed in publication [18], see Eq. 4

$$p_s = \frac{0.754}{Z} + \frac{2.457}{Z^2} + \frac{6.5}{Z^3} = 1.773 \quad (4)$$

**Step 5:** Find peak reflected overpressure using the Rankine-Hugoniot formula for an ideal gas [28], see Eq. 5, where  $\Delta p_s = p_s \cdot p_0 = 1.773 \cdot 0.1 = 0.180$  MPa is the free air blast overpressure.

$$\Delta p_r = 2\Delta p_s + \frac{6\Delta p_s^2}{\Delta p_s + 7p_0} = 0.579 \text{ MPa} \quad (5)$$

**Step 6:** Find duration of the blast wave according to the Sadovskiy formula [18], see Eq. 6.

$$\tau^+ = 1.5 \cdot \sqrt{Z} \cdot \sqrt[3]{m} = 0.898 \text{ ms} \quad (6)$$

**Step 7:** Find change in time of the overpressure according to the Liu and Chiu formula [13], see Eq. 7, where  $a = 1.39 \cdot \Delta p_s^{0.54}$ .

$$\Delta p(t) = \Delta p_r \left( 1 - \frac{t}{\tau^+} \right) e^{\left( -\frac{at}{\tau^+} \right)} \quad (7)$$

### 3. Sandwich panel subjected to fragment impacts

The six spherical bullets attached to the charge unit, see Fig. 1, were accelerated by a blast wave. This part of the investigation aimed to determine the fragment trajectories, fragment velocities, fragment spread zones, and the size of the inlet and outlet holes. Note that the size of the fragments is small enough to not influence the deflection of the sandwich panel.

Regarding the fragment trajectories, it was noted that they

could be described as straight lines. The velocity of fragments before and after penetration through the sandwich panel was calculated from the position of the fragment on the recorded movie frames, the point of perforation of the sandwich panel and the measured flight time. Taking into account the above, the average velocity of the fragments before perforation and after penetration was 386.0 m/s and 285.4 m/s, respectively. In the

case of the fifth test where two stacked sandwich panels were considered, the fragment velocity after penetration through the sandwich panels was reduced to 169.2 m/s. Stacking two panels together reduced fragment velocity by 2.17 times more than the reduction revealed for one sandwich panel. In Figure 5 the fragment traces through the core layers are depicted.

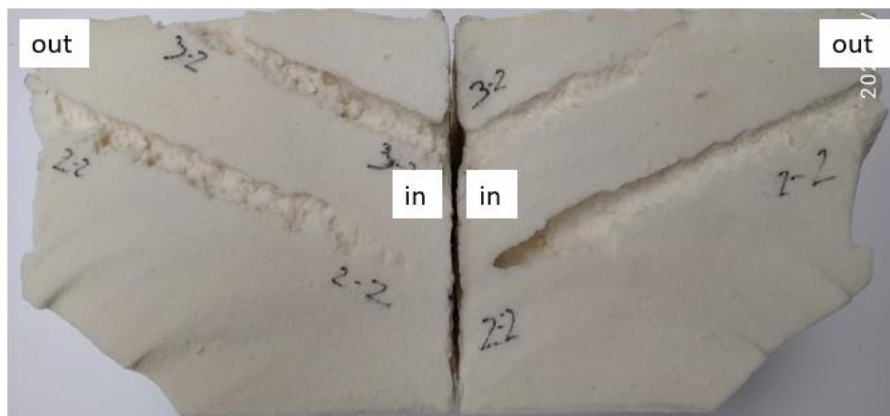


Fig. 5. Fragment traces along the core layer (arrows represent the direction of the fragment flight).

Note that they are represented by straight lines. This phenomenon can be justified by the negligible influence on the fragment flight of both the gravity and the anti-penetration ability of the core layer. Therefore, the fragment trajectories and velocities in the presented tests depend only on the pressure imposed on the fragment by the blast. Some of the fragments missed the horizontal obstacle due to its rectangular size. The

average percentage of fragment impacts on the sandwich panel for five tests was 36.7% (11 impacts of 30 possible). The distribution of fragment impacts in the sandwich panel is schematically depicted in Fig. 6, where five spread zones (A1–A5) were introduced. Each spread zone can be characterized by the radius of the base cone circle  $R_{Ai}$ , the area of the zone  $A_i$  and the number of fragment impacts  $n_{Ai}$ , see Table 2.

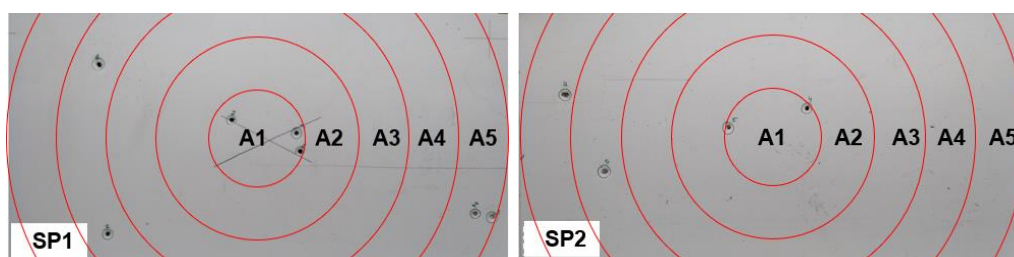


Fig. 6. Fragment spread zones.

Table 2. Fragment spread zone information.

Spread zone	Units	A1	A2	A3	A4	A5
Radius $R_{Ai}$	[cm]	10.0	20.0	30.	40.0	50.0
Area $A_i$	[cm <sup>2</sup> ]	314.2	942.5	1345.7	1119.3	1278.3
Impacts $n_{Ai}$	[-]	5	0	0	3	3

The size of the holes on the top facing (fragment inlet) and on the bottom facing (fragment outlet) is the last aspect related to the accelerated fragments which have been investigated. The inlet holes were circular or oval, while the outlet holes were oval,

triangular, or quadrilateral, see Figs. 7a and 7b, respectively. Note that the edges of the outlet holes were sharp. In Figure 7 scatter plots of the hole areas are also presented in each spread zone.

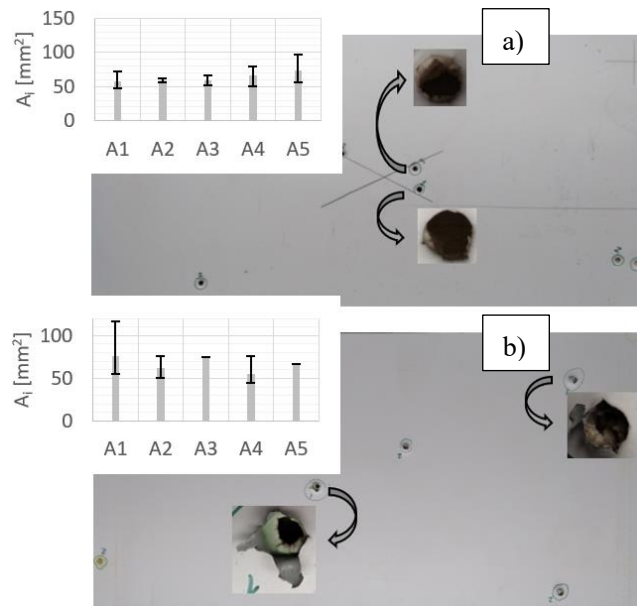


Fig. 7. Hole sizes after fragment perforation: a) top facing (fragment inlet), b) bottom facing (fragment outlet).

#### 4. Sandwich panel subjected to wave impact load

Another aspect of the research concerned the reliability of sandwich panels, understood as the ability to withstand a series of wave impact loads. In the experiment, sandwich panels were simply supported. No fasteners were used along the support line; thus, the sandwich panels were lifted during the underpressure phase. During the overpressure phase, the sandwich panels were subjected to bending and shear forces. The evolution of the failure of the repeatedly loaded SP1 panel is depicted in Fig. 8.



Fig. 8. Evolution of failure.

After the first and second tests, the sandwich panel returned to its original state after the wave impact load. In the case of the third test, the deformation was permanent. Note that the ultimate deflection should not exceed 1/100 of the span length according to serviceability limit state conditions. In our case, the maximum allowable deflection was equal to  $u_{z,(ult)} = 9.4$  mm, thus after the first and second tests (first and second wave impact load) the sandwich panel deflection was not exceeded, while after the third test (third wave impact load) the deflection limit was exceeded.

During the first test, the measured deflection,  $u_{z,(1)} = 9.17$  mm, and the shear of the core was observed in the left support (see Fig. 8a). During the second test, the core shear from the first blast load evolved and manifested as delamination of the top facings. The deflection slightly increased;  $u_{z,(2)} = 9.38$  mm. After the third test (see Fig. 8b), the core shear at the right support was observed, and the delamination of the top facing was significantly increased. This time, the deflection was considerably greater;  $u_{z,(3)} = 13.75$  mm.

#### 5. Equivalent static load

Next, the equivalent static load will be determined to assess the ultimate limit state (ULS) utilization level of the sandwich panel. Furthermore, the equivalent static load will be used in the finite element model validation process. The equivalent static load can be determined using the measured deflection of the sandwich panel. In the experiments, the simply supported sandwich panels were rectangular, with a length-to-width ratio of 1:2. In this case, the beam analogy can be used to estimate

internal forces and displacements. The sandwich panels used in the experiments are analysed using the first-order shear deformation theory (FSDT) because the core layer was made of material with a negligible Young's modulus (compared to Young's modulus of the facings). The theoretical background of the FSDT is described in [15, 25]. The basis of the FSDT for sandwich beams with flat or slightly profiled facings, according to [30], are presented below (Eq. 8 – 13) Consider that the facings transfer the normal stresses, while the core layer transfers the shear stresses: see Eq. 8, which describes the relationship between stresses and strains.

$$M_y = B_S(\gamma' - w'') \text{ and } V_z = A_C G_C \gamma \quad (8)$$

In Eq. 8,  $M_y$  represents the bending moment,  $V_z$  represents the shear force,  $B_S$  represents the flexural rigidity of the panel,  $A_C$  represents the cross-section area of the core layer,  $G_C$  represents the Kirchhoff modulus of the core layer,  $\gamma$  represents the shear strain of the core layer, and  $w$  represents the vertical deflection of the panel. The flexural stiffness of the sandwich panel  $B_S$  is the function of the facings' cross-section area ( $A_{F1}$ ,  $A_{F2}$ ), the facings' Young's modulus ( $E_{F1}$ ,  $E_{F2}$ ), and the distance ( $e$ ) between the facings' centre of gravity; see Eq. 9:

$$B_S = \frac{E_{F1} A_{F1} E_{F2} A_{F2}}{E_{F1} A_{F1} + E_{F2} A_{F2}} e^2 \quad (9)$$

Note that in the case of flat or slightly profiled facings, their second moment of area is negligible. The equilibrium equations are presented in Eq. 10

$$M_y' - V_z = 0 \text{ and } V_z' + q = 0 \quad (10)$$

where  $q$  represents the uniformly distributed load.

Table 3. Mechanical and geometrical properties of sandwich panel.

No.	Parameter	Unit	Condition / quantity / value	Comments / Symbol definition
1	$w$	[mm]	9.17 < 9.40	Deflection measured during the first test (9.17mm), Limit $L/100 = 9.4$ mm, <b>SLS satisfied</b>
2	$k$	[-]	6.94	$k = 3B_S / G_C A_C L^2$ , see Eq. 13
3	$\xi$	[-]	0.5	$\xi = x/L$
4	$L$	[mm]	940	Span length measured to the centre of the width of the supports (width of the supports is 60 mm)
5	$e$	[mm]	119.5	Distance between centroids of the facings
6	$B_S$	[Nmm <sup>2</sup> ]	3.53E+11	Flexural stiffness of the sandwich panel

Table 4. Equivalent values.

No.	Parameter	Unit	Condition / quantity / value	Comments / Symbol definition
1	$q^E$	[kN/m]	13.71	Equivalent uniformly distributed loading obtained from the reformulation of Eq. 13: $q^E = \frac{24B_S w(x)}{L^4 \left( (1 + 4k)\xi - 4k\xi^2 - 2\xi^3 + \xi^4 \right)}$
2	$M_y^E$	[kNm]	1.51	Equivalent mid-span bending moment

Substituting Eq. 8 into Eq. 10, the differential equations take the form of Eq. 11:

$$B_S(\gamma'' - w''') - A_C G_C \gamma = 0 \text{ and } A_C G_C \gamma' = -q \quad (11)$$

Resolving Eq. 11 concerning  $\gamma$  and  $w$ , we obtain the following equilibrium differential Eq. 12:

$$w^{IV} = \frac{q}{B_S} - \frac{q''}{A_C G_C} \text{ and } \gamma'' = -\frac{q'}{A_C G_C} \quad (12)$$

Having this equation for a simply supported beam with a uniformly distributed load, we can find the formula for the deflection line using Eq. 13

$$w(x) = \frac{qL^4}{24B_S} \left( (1 + 4k)\xi - 4k\xi^2 - 2\xi^3 + \xi^4 \right) \quad (13)$$

where  $L$  represents the span of the sandwich panel,  $\xi = x/L$ , and  $k = 3B_S / G_C A_C L^2$ . The maximal deflection happens when  $\xi = 0.5$ . Having the deflection at the midpoint (measured during the experiment) and using Eq. 13, we can find the uniformly distributed load  $q$ . Table 3 presents the mechanical and geometrical properties, while Table 4 calculation of the equivalent uniformly distributed load, the equivalent internal forces, and the equivalent stresses. According to Table 3, the SLS condition is satisfied. The verification of the normal stresses at mid span (ULS verification) is also satisfied, but the shear stresses are too large thus this condition is not satisfied (see Table 4). It is in agreement with the results observed in the experiments, i.e. also only the shear failure was observed; see Fig. 8.

3	$F_F^E$	[kN]	12.67	Equivalent axial force along facings due to $M_y^E$ $F_F^E = M_y^E / e$
No.	Parameter	Unit	Condition / quantity / value	Comments / Symbol definition
4	$\sigma_F^E$	[MPa]	48.7 < 377.0	Equivalent normal tension stresses in the bottom facing at midspan $\sigma_F^E = M_y^E / A_F$ <b>ULS 1 satisfied</b>
5	$\sigma_F^E$	[MPa]	48.7 < 118.9	Equivalent normal compression stresses in the top facing at midspan $\sigma_F^E \leq \sigma_{crit}$ , $\sigma_{crit} = 0.794 \cdot (E_F \cdot E_C \cdot G_C)^{1/3} = 118.9$ MPa, (see [30]) <b>ULS 2 satisfied</b>
6	$V_z^E$	[kN]	6.44	Equivalent shear force at the support
7	$\tau_C^E$	[MPa]	0.108 > 0.075	Equivalent shear stresses in the core layer $\tau_C^E = V_z^E / A_C$ <b>ULS 3 failed</b>

## 6. Numerical simulations

The costs of field tests are very high. They include the costs of explosives, tested materials, and the costs of ensuring safety on the training ground (the presence of a fire brigade, paramedics, and people trained to carry out operations with the use of explosives). In this case, the use of numerical simulations seems justified in the continuation of parametric research. Thus, it is necessary to validate the numerical model. The numerical simulations presented in this section were conducted in Abaqus/CAE [1]. The finite element approach consisted of the following three steps: the validation of the finite element model using the equivalent static load, the simulation of the blast wave load, and the simulation of the ball penetration through the sandwich panel. Schematically, the three-step FE approach is presented in Fig. 9. In all three FE approaches the whole sandwich panel was modelled. The numerical model consisted of the sandwich panel, the two steel supports, and the spherical bullet (at third step, see Fig. 9). All considerations refer to the sandwich panel with a continuous core layer, i.e. panel A (PIR foam core). The facings (modelled using shell finite elements) of the sandwich panel were numerically bonded with the core (modelled using solid finite elements) using tie contact. The used tie contact definition allowed for bonding two surfaces with different mesh densities. The contact between bottom facing of the sandwich panel and the steel pad supports were defined in the FE model as “hard contact”, therefore, the penetration of the slave body is minimized in respect to the master body.

The contact pressure appears when the clearance is equal 0. Also, this type of contact technique assumes no limit of contact

pressure. The “hard contact” with the introduced friction coefficient equal 0.3 allows for separation between the sandwich panel and the support.

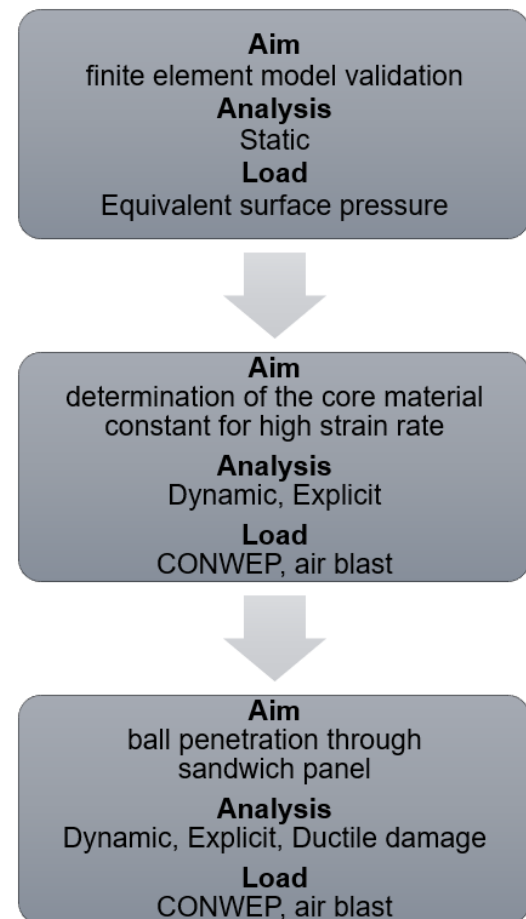


Fig. 9. Three-step FE approach in Abaqus/CAE.

This contact definition corresponds to the situation at the field where the sandwich panel was freely placed on the supports. Note that in the FE model, the simplified shape of the supports was assumed with the constrained all translational and all rotational degrees of freedom applied to the bottom surface

of the steel pad. Step one (static) was solved using Newton solution techniques, while steps two and three (explicit dynamic) were solved using an explicit central-difference time integration

rule. In Table 5 the definition of finite element types, mesh sizes, and material models are depicted.

Table 5 Basic information of the finite element model

No.	FE part	FE type	FE name	Mesh sizes [m]	Material model
1	Facings	Shell	S4*	0.02, 0.0005	elastic-plastic, isotropic, ductile damage
2	Core	Solid	C3D8I**	0.02	elastic, isotropic
3	Ball	Solid	C3D10M***	0.004	elastic, isotropic

\* 4-node doubly curved thin or thick shell, hourglass control, element deletion active in steps two and three

\*\* 8-node linear brick, incompatible modes, hourglass control

\*\*\* 10-node modified quadratic tetrahedron

### 6.1 The first step of the numerical analysis

In the first step, the equivalent static load was used. In that case, the sandwich panel was subjected to the equivalent surface load  $q^E/b = 13.71 \text{ kN/m} / 0.5 \text{ m} = 27.42 \text{ kN/m}^2$  applied along the top facing. The results of step one of the numerical analyses are depicted in Fig. 10. These FE results (first step – equivalent surface load) are compared with the experiment and analytical

calculations obtained using FSDT, see Table 6. The data summarised in Table 6 show that the stress values of the numerical model are consistent with those calculated using FSDT. The differences do not exceed 2%. Furthermore, it is worth noting that the value of the deflection of the slab obtained by the numerical model is underestimated in relation to the actual deflection by 0.8%.

Table 6. Comparison of the results – equivalent load concept FSDT vs. FE analysis.

No.	Measured value	Experiment	FSDT	FE model	Percentage difference	
					Exp./FSDT	Exp./FEM
1	Mid-span deflection $u_z$ [mm]	9.17	9.17	9.10	0%	0.8%
2	Mid-span normal stresses in facings $\sigma_x$ [MPa]	–	48.7	49.07	–	–0.8%
3	At the support shear stresses in core $\tau_{xz}$ [MPa]	–	0.108	0.110	–	–1.9%

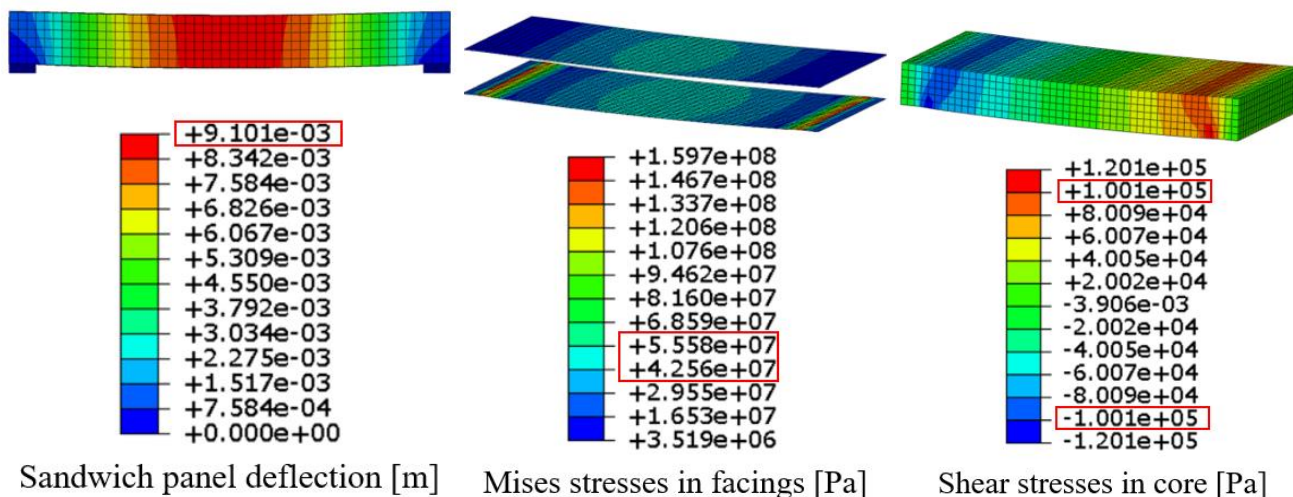


Fig. 10. Results of the FE analysis – step one.

### 6.2 The second step of the numerical analysis

The second step of the numerical analysis was to find the accurate flexural stiffness of the sandwich panel when exposed to blast load. The blast load (air blast) was defined using CONWEP (Conventional Weapon Effects Programme

implemented in Abaqus/CAE [1]). The 'standoff' distance  $H = 0.85 \text{ m}$  and the charge size  $m = 75 \text{ g}$  were assumed according to field tests. The flexural stiffness of the sandwich panel  $B_S$  depends on the stiffness of the facings; and the stiffness of the core layer ( $G_C$  – Kirchhof modulus) with the introduced  $k$

parameter; see Eq. 9 and Table 3. Because Young's modulus of the steel facings remains unchanged during the high strain rates (the yield and ultimate strength increase only) we decided not to use the Johnson-Cook plasticity model (in the experiment the sandwich panel failed due to the shear stresses). Only the properties of the core layer ( $G_c$ ) change during the high strain rate, which influences the overall stiffness of the sandwich panel  $B_s$ . To find the value of the Kirchhoff modulus for a high strain rate, an iteration procedure was implemented. As a result, the modified Kirchhoff modulus was determined,  $G_c^{mod} = 9.65$  MPa.

### 6.3 The third step of the numerical analysis

The third step of the numerical analysis covers the investigation of the fragment that perforates the sandwich panel. The material model used in this step comprises the findings from step two ( $G_c^{mod}$ ), and it is enhanced by the incorporated ductile damage model for steel facings. Since the trajectories of the fragments along the layer are represented by the straight lines; see Fig. 5, the damage of the core layer will not be defined while the fragment penetration is investigated. Ductile damage requires the definition of equivalent fracture strain at the time of damage initiation, stress triaxiality, equivalent plastic strain rate, and displacement damage evolution. To obtain these data, the stress-strain curve from the static tensile test of the facings are used. In Figure 11, the thin grey lines represent the strain-stress curves for individual specimens, while the thick black line represents the mean strain-stress relation that will be used to define the data for ductile damage in Abaqus/CAE.

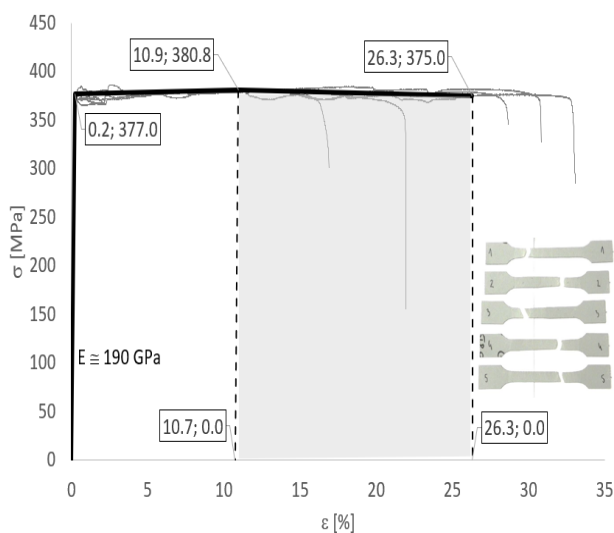


Fig. 11. Stress-strain curves of sandwich panel facings material

In Figure 11 the equivalent fracture strain at damage initiation is depicted ( $\varepsilon_{eq} = 0.107$ ). The initiation of the equivalent fracture strain damage refers to the ultimate stress along the stress-strain curve. According to the Abaqus/CAE documentation [1], stress triaxiality is defined as

$$\eta = -\frac{p}{q} \quad (14)$$

where  $q$  represents the equivalent Mises stress ( $\sigma_M$ ) and  $-p$  represents the hydrostatic pressure stress, i.e. 1/3 trace of the stress tensor, see Eq. 15

$$-p = \frac{1}{3} \cdot \text{trace}(\mathbf{T}) = \frac{1}{3} \cdot (\sigma_{xx} + \sigma_{yy} + \sigma_{zz}) \quad (15)$$

Since, stress-strain curve used in this research represents the uniaxial tension the stress triaxiality factor takes the following form

$$\eta = \frac{\frac{1}{3} \cdot (\sigma_{xx} + \sigma_{yy} + \sigma_{zz})}{\sigma_M} = \frac{\frac{1}{3} \sigma_{xx}}{\sigma_{xx}} = \frac{1}{3} \quad (16)$$

Since, the stresses in the samples in the experiment are much below yield point level the equivalent plastic strain rate parameter will be neglected in FE analysis. The last parameter represents the displacement damage which can be calculated from the Eq. 17 and represents the plastic displacement after damage initiation

$$\bar{u}_f^{pl} = \frac{2G_f}{\sigma_{y0}} = 1.55 \cdot 10^{-5} [m] \quad (17)$$

In Equation (17)  $\sigma_{y0}$  represents the ultimate stress and  $G_f$  represents the fracture energy which can be calculated as an area  $A_f$  below the stress-strain curve (see the shaded area in Fig. 11) multiply the characteristic finite element length  $l_c$ . In our case, the  $l_c$  is taken 0.0005m which corresponds to the size of the mesh in the area where the fragment impact is expected, while the regular mesh size over the facings was 0.02m. Note that the mesh size of 0.0005m was chosen after the convergence analysis. Along the area where the fragment impact is expected the five different mesh sizes were investigated, see Table 7.

Table 7. Convergence analysis with respect to mesh size – fragment penetration case.

Task no.	Mesh size [mm]	Ball/facing mesh ratio	Velocity after penetration [m/s]			Taks size		
			Experiment	FE model	Difference	CPU time [h]	No. of elements	No. of nodes
1	0.25	12.00	285.4	305.33	-6.98%	20.89	89371	192889
2	<b>0.50</b>	<b>6.00</b>		<b>304.60</b>	<b>-6.73%</b>	<b>1.61</b>	<b>38201</b>	<b>141696</b>
3	1.00	3.00		311.10	-9.01%	0.36	27633	131154
4	2.00	1.50		316.77	-10.99%	0.22	25335	128885
5	4.00	0.75		128.91	54.83%	0.18	24067	127616

According to the results presented in Table 7, the 0.50mm mesh size was used in the area where the impact was expected for further investigations. The 0.5mm mesh size provides the best fit with the experiment – the fragment velocity after penetration was calculated with 6.73% overestimation. Note that the use of a smaller mesh size significantly extends (13 times) the computation time without improving the convergence with experiment. In Figure 12 the penetration of the fragment in the FE model is presented.

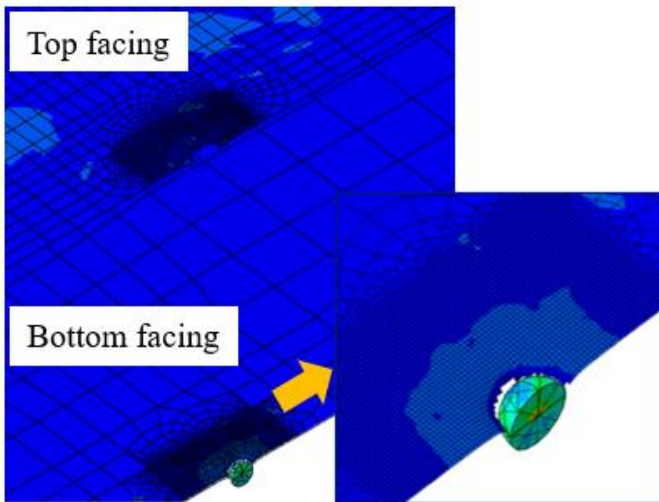


Fig. 12. Spherical ball (fragment) penetration obtained in the FE model (the core layer is only excluded from the viewport).

A numerical experiment was conducted to assess the effect of fragment size on its penetration capabilities. Balls with a linearly varying diameter from 5mm to 8mm (change in 0.5mm increments) were analysed. The graph in Fig. 13 shows the change in velocity of the balls after they pass through the sandwich panel. One can note that the change of the velocity is exponential, that corresponds to the change of the mass of the fragments.

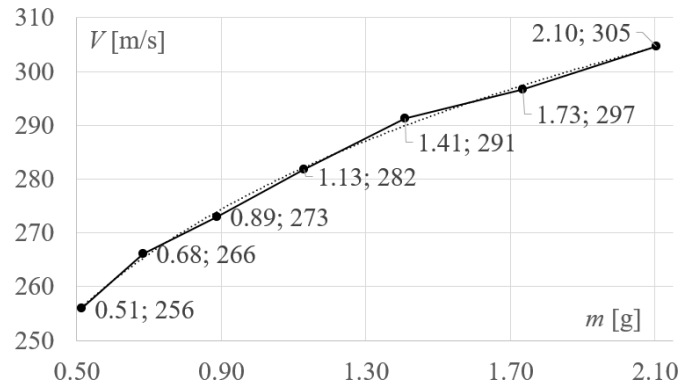


Fig. 13. Change of the velocity after sandwich panel penetration with respect to various mass of the fragment.

In Figure 14 the time history plots are presented depicting, for various ball diameters, the change of velocity after penetration of the sandwich panel. Note that the velocity of the ball after penetration of the sandwich plate "numerically" stabilised around the characteristic, for a ball of a given mass, velocity given in the diagram.

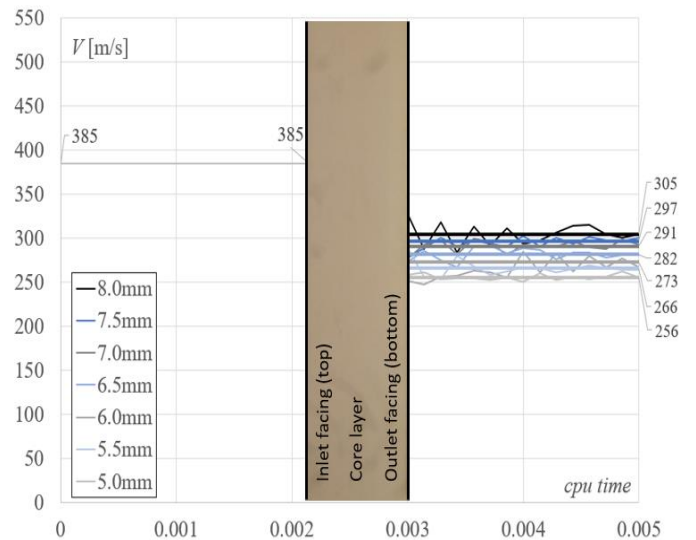


Fig. 14. Time history plots of balls of various diameter depicting change of velocity after penetration of the sandwich panel.

## 7. Concluding remarks

The paper presents new and original experimental results of sandwich panels used in civil engineering, which were subjected to blast load (wave impact load) and fragment impact. On the basis of the experimental research, we can formulate the following conclusions. The study shows that fragments (of a weight 2.1 g each) trajectories, spread zones, and velocities depend only on the pressure imposed on the fragment by the blast wave. It was revealed that sandwich panels with metallic thin facings and soft core have poor antipenetration abilities.

The validation of the finite element model was successfully obtained using the determined – from First Order Shear Deformation Theory – equivalent static load. The presented calculation of the equivalent static load was based on the

measured deflections in the experiment. The internal forces from the equivalent static load indicated and confirmed the observed failure mechanisms of the sandwich panels subjected to a blast load, that is, the shear of the core layer. Furthermore, the introduced definition of ductile materials, which requires data from tensile tests, allows the simulation of the bullet through the sandwich panel. The finite element model of sandwich panel perforation due to accelerated fragments and subjected to blast wave was validated based on mid-span deflections and outlet velocity comparison to the field test results. The numerical modeling enabled computing the outlet velocities for smaller masses/sizes of debris. In conclusion, such a procedure can be thought helpful in practical engineering design.

## Acknowledgments

This research was funded by the National Centre for Research and Development, Poland, under the grant DOB-BIO10/01/02/2019 within the Defence and Security Programme

## References

1. Abaqus 2016 documentation: <http://130.149.89.49:2080/v2016/index.html>. access 12.12.2022.
2. Alberdi R. Przywara J. Khandelwal K. Performance evaluation of sandwich panel systems for blast mitigation. *Engineering Structures* 2013; 56: 2119–2130. <http://dx.doi.org/10.1016/j.engstruct.2013.08.021>.
3. Al-Rifaie H. Studziński R. Gajewski T. Malendowski M. Peksa P. Sumelka W. Sielicki PW. Full scale field testing of trapezoidal core sandwich panels subjected to adjacent and contact detonations. *Modern Trends in Research on Steel, Aluminium and Composite Structures: Proceedings of the XIV International Conference on Metal Structures (ICMS2021)*. Poznan, Poland, 16–18 June 2021. Leiden, Netherlands: Routledge, 2021 - s. 393–399. <https://doi.org/10.1201/9781003132134-50>.
4. Al-Rifaie H. Studziński R. Gajewski T. Malendowski M. Sumelka W. Sielicki PW. A new blast absorbing sandwich panel with unconnected corrugated layers— numerical study. *Energies* 2021; 14(1). <https://doi.org/10.3390/en14010214>.
5. Brekken KA. Reyes A. Berstad T. Langseth M. Børvik T. Sandwich panels with polymeric foam cores exposed to blast loading: an experimental and numerical investigation. *Appl Sci* 2020;10: 9061. doi:10.3390/app10249061.
6. Cheng W. Bin X. Yuen SCK. Numerical analysis of cladding sandwich panels with tubular cores subjected to uniform blast load. *International Journal of Impact Engineering* 2019;133:103345. <https://doi.org/10.1016/j.ijimpeng.2019.103345>.
7. Ebrahimi H. Vaziri A. Metallic sandwich panels subjected to multiple intense shocks. *International Journal of Solids and Structures* 2013;50:1164–1176. <https://doi.org/10.1016/j.ijsolstr.2012.12.013>.
8. Estrada Q. Szwedowicz D. Majewski T. Martinez E. Rodriguez-Mendez A. Effect of quadrilateral discontinuity size on the energy absorption of structural steel profiles. *Eksploatacja i Niezawodność – Maintenance and Reliability* 2016; 18 (2):186–193. <https://doi.org/10.17531/ein.2016.2.5>.
9. Ferdynus M. Kotelko M. Kral J. Energy absorption capability numerical analysis of thin-walled prismatic tubes with corner dents under axial impact. *Eksploatacja i Niezawodność – Maintenance and Reliability* 2018; 20(2): 252–259. <https://doi.org/10.17531/ein.2018.2.10>.
10. Iluk A. Method of evaluating the stiffness of a vehicle with respect to the risk of explosion. *Eksploatacja i Niezawodność – Maintenance and Reliability* 2014; 16 (2): 224–228.
11. Jackson M. Shukla A. Performance of sandwich composites subjected to sequential impact and air blast loading. *Composites: Part B* 2011;42:155–166. <https://doi.org/10.1016/j.compositesb.2010.09.005>.

12. Komorek A. Przybyłek P. Examination of the influence of cross-impact load on bend strength properties of composite materials. used in aviation. *Eksploatacja i Niezawodność – Maintenance and Reliability* 2012; 14 (4): 265–269.
13. Lee JHS. *Physics of explosion*. Montreal: McGill University; 1984.
14. Li Y. Lv Z. Wang Y. Blast response of aluminum foam sandwich panel with double V-shaped face plate. *International Journal of Impact Engineering* 2020;144:103666. <https://doi.org/10.1016/j.ijimpeng.2020.103666>.
15. Reddy JN. A simple higher-order theory for laminated composite plates. *J Appl Mech* 1984;51:745–752. <https://doi.org/10.1115/1.3167719>
16. Rolfe E. Kelly M. Arora H. Hooper P. Dear JP. Failure analysis using X-ray computed tomography of composite sandwich panels subjected to full-scale blast loading. *Composites Part B* 2017;129:26–40. <http://dx.doi.org/10.1016/j.compositesb.2017.07.022>.
17. Sachs RG. *Dependence of blast on ambient pressure and temperature*. Aberdeen: BRL-466 Ballistic Research Laboratory; 1944. <https://doi.org/10.21236/ADA800535>
18. Sadovskiy MA. Mechanical effects of air shockwaves from explosions according to experiments. In: Sadovskiy MA. editor. *Geophysics and physics of explosion*. Moscow: Nauka Press; 2004. Russian.
19. Shen J. Lu G. Zhao L. Qu Z. Response of curved sandwich panels subjected to blast loading. *Journal of Performance of Constructed Facilities* 2011;25. 5:382–393. [https://doi.org/10.1061/\(ASCE\)CF.1943-5509.0000234](https://doi.org/10.1061/(ASCE)CF.1943-5509.0000234).
20. Sielicki P.W.; Stachowski. M. Implementation of Sapper-Blast-Module. a Rapid Prediction Software for Blast Wave Properties. *Cent. Eur. J. Energetic Mater.* 2015. 12. 473–486.
21. Studziński R. Gajewski T. Malendowski M. Sumelka W. Al-Rifaie H. Peksa P. Sielicki PW. Blast test and failure mechanisms of soft-core sandwich panels for storage halls applications. *Materials* 2021;14(1):70. <https://doi.org/10.3390/ma14010070>.
22. Sun G. Wang E. Zhang J. Li S. Zhang Y. Li Q. Experimental study on the dynamic responses of foam sandwich panels with different face sheets and core gradients subjected to blast impulse. *International Journal of Impact Engineering* 2020;135:103327. <https://doi.org/10.1016/j.ijimpeng.2019.103327>.
23. Szudrowicz M. Layered composite increasing the resistance of patrol and intervention vehicles to the impact of improvised explosive devices (IED) from below. *Eksploatacja i Niezawodność – Maintenance and Reliability* 2018; 20(1): 9–15. <https://doi.org/10.17531/ein.2018.1.2>.
24. Szymczak T. Kowalewski ZL. Strength tests of polymer-glass composite to evaluate its operational suitability for ballistic shield plates. *Eksploatacja i Niezawodność – Maintenance and Reliability* 2020; 22 (4): 592–600. <http://dx.doi.org/10.17531/ein.2020.4.2>
25. Timoshenko SP. On the correction for shear of the differential equation for transverse vibrations of prismatic bars. *Phil Mag Ser* 1921;6. 41:744–746. <https://doi.org/10.1080/14786442108636264>
26. Ullah A. Ahmad F. Jang H.-W. Kim S.-W. Hong J.-W. Review of analytical and empirical estimations for incident blast pressure. *KSCE J Civ Eng* 2017;21:2211–2225. <https://doi.org/10.1007/s12205-016-1386-4>.
27. Wadley HNG. Børvik T. Olovsson L. Wetzel JJ. Dharmasena KP. Hopperstad OS. Deshpande VS. Hutchinson JW. Deformation and fracture of impulsively loaded sandwich panels. *Journal of the Mechanics and Physics of Solids* 2013;61:674–699. <http://dx.doi.org/10.1016/j.jmps.2012.07.007>.
28. Yin X. Gu X. Lin F. Kuang X. Numerical analysis of blast loads inside buildings. In: Yuan Y. Cui J. Mang HA. editors. *Computational structural engineering*. Dordrecht. The Netherlands: Springer; 2009. p. 681–690. [https://doi.org/10.1007/978-90-481-2822-8\\_74](https://doi.org/10.1007/978-90-481-2822-8_74).
29. Yuen S.C.K. Nurick G.N. Theobald M.D. Langdon G.S. Sandwich Panels Subjected to Blast Loading 2009; In: Shukla A., Ravichandran G., Rajapakse Y. (eds) *Dynamic Failure of Materials and Structures*. Springer. Boston. MA. [https://doi.org/10.1007/978-1-4419-0446-1\\_10](https://doi.org/10.1007/978-1-4419-0446-1_10).
30. Zenkert D. *An introduction to sandwich structures*. Stockholm: Engineering Materials Advisory Services; 1995.
31. Zhang Ch. Cheng Y. Zhang P. Duan X. Liu J. Li Y. Numerical investigation of the response of I-core sandwich panels subjected to combined blast and fragment loading. *Engineering Structures* 2017;151:459–471. <https://doi.org/10.1016/j.engstruct.2017.08.039>.
32. Zhang P. Cheng Y. Liu J. Li Y. Zhang Ch. Hou H. Wang Ch. Experimental study on the dynamic response of foam-filled corrugated core sandwich panels subjected to air blast loading. *Composites Part B* 2016;105:67–81. <http://dx.doi.org/10.1016/j.compositesb.2016.08.038>.
33. Zhou X. Jing L. Deflection analysis of clamped square sandwich panels with layered-gradient foam cores under blast loading. *Thin-Walled Structures* 2020;157:107141. <https://doi.org/10.1016/j.tws.2020.107141>.